

Imitate and optimize modern control algorithms for forestry cranes by means of artificial neural networks

Marco Wydra, Andreas Bauer, Chris Geiger, Marcus Geimer

Modern hydrostatic function drives for agricultural and forestry machines require complex control algorithms. Electric controls offer significant energy and control advantages over the state of the art, such as reduced tendency to oscillate or implementation of a variable power limitation. Therefore, new algorithms are essential for sustainable optimization of future machines. The paper investigates a method to automatically transfer an existing control algorithm to an artificial neural network (ANN), which will be optimized by the Pattern Search algorithm afterwards. The method was applied to a forestry crane with an electro-hydraulic flow-on-demand control. After 41 generations of optimized parameter sets, the ANN control already shows a behavior comparable to the reference control. With this approach it is possible to transfer deterministic algorithms into stochastic algorithms with comparable transfer functions, which can then be optimized using machine learning methods.

Keywords

Artificial neural networks (ANN), electro-hydraulic flow-on-demand control (eBSS), independent metering, forwarder, agricultural machinery

Oil hydraulic drives have been an integral part of agricultural and forestry machinery for decades. Hydrostatic drives are used for both traction drive and function drive (GEIMER and POHLANDT 2014). In this paper hydrostatic drives for the working function of forestry machines are considered. Due to socio-ecologically motivated optimization of technical systems and the electrification of machines, the development and use of energy-efficient drive systems is gaining in importance. The aim is to reduce pollutant emissions (HÄNEL et al. 2015) and increase the operating time of machines. Especially with regard to battery-powered machines, locally installed energy resources are limited due to low energy density (ALTENBURG et al. 2017). Numerous international research projects already investigated a wide variety of approaches to increase the efficiency of hydrostatic function drives in mobile machinery (ESDERS 1996, ERIKSSON 2010, AXIN 2013, DENGLER 2015, VUKOVIC et al. 2017, ZHANG et al. 2019). Many of the solutions presented have in common that the system complexity, including their control tasks, increases compared to the state of the art. So, suitable algorithms have to be developed. Approaches from topics like autonomous driving, medical technology or image recognition and processing indicate a trend towards the use of artificial intelligence (AI) (BUXMANN and SCHMIDT 2019).

The aim of this paper is to show a method to imitate existing control algorithms by means of artificial neural networks (ANN). First an ANN will be trained by supervised learning and then optimized by reinforcement learning. The use of the method is shown for an electro-hydraulic flow-on-demand control (eBSS) with independent metering. A comparison to the state of the art for hydrostatic func-

tion drives in agricultural and forestry machines shows the energy saving potential for this complex control strategy. Finding a solution is presented, verified and finally discussed on the basis of a forestry crane. For this purpose, the control task is named, significant changes in the hydraulic system are shown and different control algorithms are tested and compared using the MOBIL method (POHLANDT 2018).

Hydrostatic function drives in agriculture

The hydrostatic function drive of a forestry crane and other agricultural machines is usually operated as a valve control system with applied pressure or flow rate (BACKÉ and BAUM 2013). A pump provides necessary hydraulic power for the hydraulic circuit in form of pressure p and flow rate Q . Actuators with linear as well as rotary motion convert hydraulic power into mechanical power. Valves between pump and actuator(s) adjust both pressure and flow rate to the demand. In modern hydraulic function drives, proportionally adjustable directional valves are used for power adjustment (FINDEISEN 2006).

The advantage of simultaneously adjusting meter-in and meter-out oil flow of an actuator is the reduced effort to realize a stable and robust control system. In addition, these directional valves can be manufactured simply and cost-effectively. The limitation of control possibilities due to mechanically coupled meter-in and meter-out flow rate as well as the way of power supply lead to significant power losses in partial load operation, see below. Each power loss increases the consumption of primary energy. So, its reduction contributes to sustainable improvement of the entire system.

RENIUS (2019) divides valve control systems in open center systems (OCS) and closed center systems (CCS). OCS are usually applied with a constantly driven pump without adjustment, so that the maximum flow rate Q_{\max} is constantly delivered. If the directional valves are not actuated, the oil can flow with less pressure losses back into the tank via a neutral circuit. CCS are characterized by the fact that in zero position the directional valves have no neutral circuit. Therefore, the flow rate must either be variably adjusted or diverted through a separate bypass. Among others, CCS are operated as constant pressure systems (CPS) or as load-sensing systems (LSS) (Figure 1).

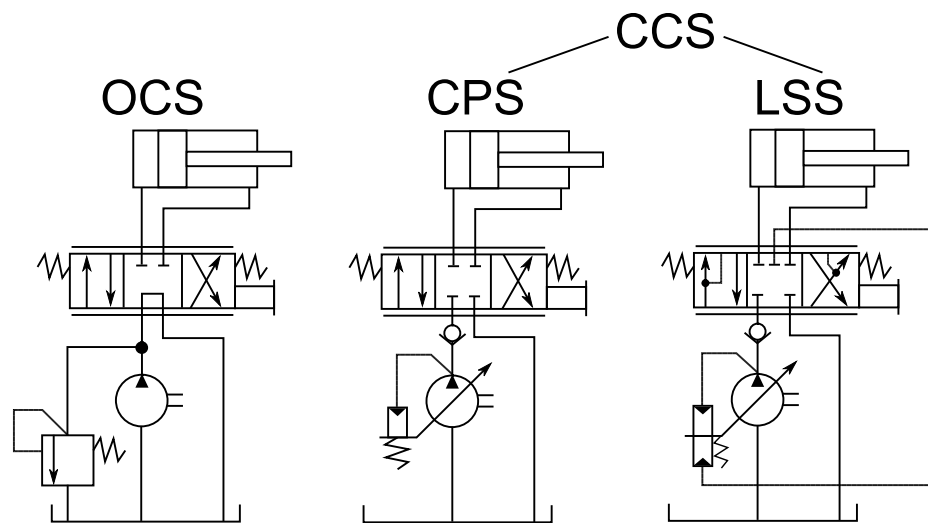


Figure 1: Schematic diagram of different hydraulic controls; according to RENIUS (2019)

In OCS the pump pressure p_p is calculated by the sum of the highest actuator pressure $p_{L,max}$ and the pressure losses at the directional valve Δp_{DV} . In CPS p_p is hold to a fixed maximum pressure value p_{max} . In LSS p_p goes by the highest actuator pressure $p_{L,max}$ plus Δp_{DV} and a constant LS control pressure difference Δp_{LS} . The value Δp_{LS} is typically approx. 20 to 30 bar depending on the operating point and system (SCHERER 2015).

The electro-hydraulic flow-on-demand control (eBSS) considered in this paper represents an alternative drive technology to the state of the art. (SCHERER 2015) describes the mode of operation and lists advantages and disadvantages. Comparable to OCS, in eBSS systems p_p depends on $p_{L,max}$ and Δp_{DV} . For the actuator with highest load, the pressure loss from pump via directional valve of the main control block is then only approx. 8 to 10 bar.

To be able to compare the power requirements of the four systems, the hydraulic pump power P_p is calculated. The hydraulic power is generally calculated as product of a pressure difference Δp and the flow rate Q (Equation 1). Losses through fittings or pipes can be considered and calculated with $\Delta p_{L,other}$

$$P = \Delta p \cdot Q \tag{Eq. 1}$$

In Figure 2 the relationship between the provided pump power, the actuator power and losses are shown graphically using a p - Q diagram. The pump power is calculated by the product of $\Delta p = p_p - p_T$ and Q_p . It represents the total area in Figure 2. The white areas represent the effective power of two actuators with different pressure levels $\Delta p_{A,n} = p_n - p_T$; $n = 1,2$ and their flow rate demand $Q_{A,n}$; $n = 1,2$. The difference between pump power and actuator power (grey) represents throttle losses in the system. These throttle losses can be divided into system inherent pressure losses Δp_L , losses at the directional valve Δp_{DV} and losses due to the LS control pressure difference Δp_{LS} . On one hand, system inherent pressure losses always occur when the pressure levels between actuators operated in parallel are not the same and high-pressure must be throttled down to actuator level. On other hand, Δp_L is unused pump power like shown in Figure 2, OCS, right hand side. It can be seen that the potential for energy-efficient operation is highest for the eBSS compared to other systems mentioned above. Also, it is independent of the operating point. SCHERER (2015) estimates a saving potential with eBSS up to 14% compared to a hydraulic-mechanical LSS.

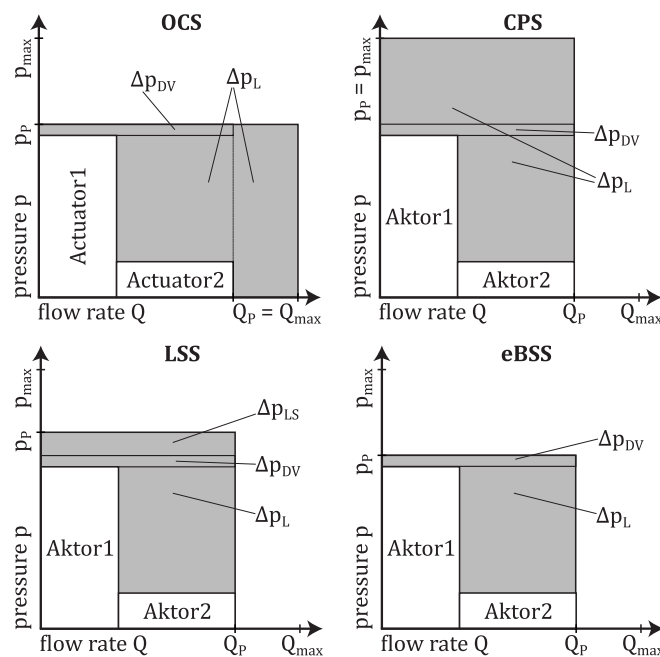


Figure 2: p - Q diagrams of the OCS, CPS, LSS and eBSS system; Losses from pipes or similar $\Delta p_{L,other}$ are not shown in the diagram; according to SCHERER (2015)

Requirements on control engineering

The actuator velocity v_n is set by the user via the control of the directional valves in the main control block. Controlling these directional valves causes opening of metering edges. Due to the pressure difference between actuator pressure p_A and pump or tank pressure $\Delta p_{ME,n} = p_p - p_{A,n} \mid p_{A,n} - p_T$ flow rate Q_n arises. The pressure level p_A of an actuator is primarily determined by load. The load can act in direction of movement (active loads) or against it (passive loads). Passive loads are supported by the pump. Active loads have a self-accelerating effect and can lead to an unintended reaction of the actuator, which can evoke an unsuitable operation behavior for the operator. A suited control should avoid that (STEINDORFF 2010).

The outgoing flow rate Q_{out} of a hydraulic cylinder is ideally determined on the cylinder surface $A_{Cyl,out}$ for a known actuator velocity v . Thus, according to Equation 2, the metering edges flow surface $A_{out}(y)$ and the pressure difference across the meter-out edge Δp_{out} are left as control variables for v . Flow coefficient α_D and oil density ρ are assumed to be constant. y represents the displacement of valve spool.

$$A_{Cyl,out} \cdot v = Q_{out} = \alpha_D \cdot \sqrt{\frac{2}{\rho}} \cdot \sqrt{\Delta p_{out}} \cdot A_{out}(y) \quad (\text{Eq. 2})$$

According to Equation 2, a self-acceleration of the actuator due to active loads can be avoided under following condition: necessary pressure difference at meter-out edge for movement is greater than load pressure $\Delta p_{out} > p_A - p_T$. Then, the necessary pressure difference Δp_{out} for the required flow rate Q_{out} is composed of load pressure p_A and a pressure difference additionally set by the pump $\Delta p_+ = \beta \cdot (p_p - p_A)$. Δp_+ acts on the outlet surface of the actuator, so pump pressure needs to be multiplied by transform factor β . For a differential cylinder β is the ratio of the two surfaces $A_{Cyl,in}$ to $A_{Cyl,out}$. For double rod cylinders or rotary drives $\beta = 1$.

Commercially available solutions to prevent actuators from self-accelerating due to active loads are specific geometry of $A_{out}(y)$ of directional valves or the use of lowering brake valves (LBV) between main control block and actuator. In order to prevent self-accelerating at any operating point by adjusting valve spool geometry $A_{out}(y)$, the design results in a high dynamic pressure Δp_{out} . So, active loads are always handled like passive loads by the system. For valves with a fixed ratio between meter-in and meter-out edge, this is an obvious and cost-effective solution. From an energy point of view, for partial load operation this is the most inefficient of the two solutions mentioned above. Even for small loads, a high pump pressure p_p is necessary due to Δp_+ .

Figure 3 shows the symbol of an LBV. When the cylinder extends, the oil flows via the check valve from main control block 1 to cylinder port A. If the cylinder retracts under load, a pressure arises in the connection from main control block 2 to cylinder port B to open the LBV. After exceeding a threshold, oil can flow from cylinder port A to main control block 1. The control pressure Δp_+ required to open the LBV is provided by the pump. A pressure intensification reduces the required pressure level of the pump. In this case $A_{out}(y)$ of the directional valve in the main control block is designed to minimize throttling losses. By reducing p_p at equal Q_p the required pump power is reduced and the system becomes more energy-efficient. Due to its design, the hydraulic-mechanically operated LBV can only operate with low vibration at specific operating points. Applied to entire working range, designing proves to be a challenge for developers (ROCCA 2003). Both, use of an adjusted valve spool geometry and use of a LBV represent the state of the art for hydrostatic function drives in agricultural and forestry machines.

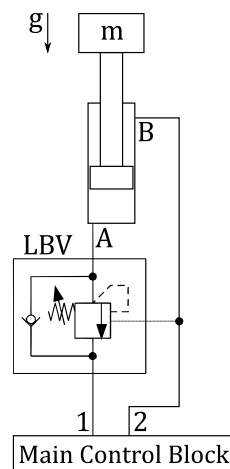


Figure 3: Structure of a system with lowering brake valve; according to Rocca (2003)

Consequently, an energy optimization for controlling active loads independent of operating point is not feasible with the current state of the art. Investigation show that independent meter-in and meter-out control is a possible solution. Control algorithms for function drives with independent metering have been investigated in literature extensively. Exemplary named are ERIKSSON(2010), AXIN (2013) and KOLKS and WEBER (2016). WEISS and WYDRA (2019) show that active loads can be controlled in an energy-efficient way using independent metering. Depending on actuator and load case, potential savings compared to state of the art can be up to 80%. Further, a modified control strategy of the control system described in WYDRA et al. (2017) is applied. This control strategy will be referred to as Reference Control.

Application, reference cycle and research object

The operating ratio of hydrostatic function drive and traction drive of a mobile machine vary depending on type and application. In this paper, the function drive of a forwarder will be examined in more detail, because the portion of the forestry crane in the overall harvesting process of fresh wood determined by MANNER et al. (2016) is between 80% and 85%. The remaining operating portion is allocated to traction drive. The Power converted in hydrostatic function drive is accordingly relevant for investigations of energy efficiency and controllability. The forestry crane has six hydraulic cylinders and one rotating actuator. One hydraulic cylinder each for inner boom, outer boom, telescope and grapple. The swivel is driven by two identical hydraulic cylinders (Figure 4).

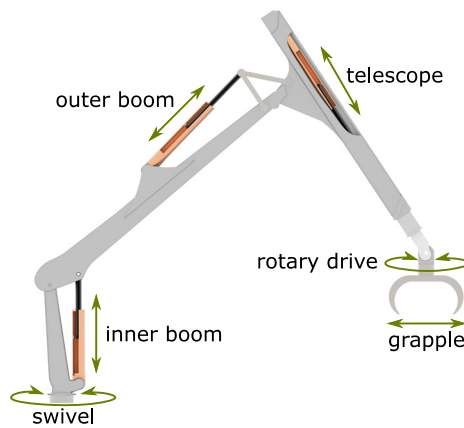


Figure 4: Representation of a forestry crane and its six cylinders and the rotary drive; according to (GEIGER und GEIMER 2017)

A load cycle according to GEIGER und GEIMER (2017) is used as reference, which describes the loading activity of a forwarder. In order to reduce complexity of the model, the rotary drive at the end of telescope and the telescope itself are not actuated in simulation. During a load cycle, the grapple is usually controlled independently of the movement of the crane tip. Therefore, time slices with simultaneous actuation of grapple and other actuators are very small. In that case, the grapple function can be neglected for the present control development and intention of investigation.

The motion sequence of the loading activity is depicted in Figure 5. As can be seen on the left hand side, the crane first moves out of stanchion basket towards tree trunk (Phase I). There the log is gripped (phase II), transported back over stanchions into stanchion basket (phase III) and deposited (phase IV). On the right hand side, associated travel paths of inner boom cylinder (IBC), outer boom cylinder (OBC) and swivel cylinders (SWC) are shown. The motion sequences were created by recording several test runs.

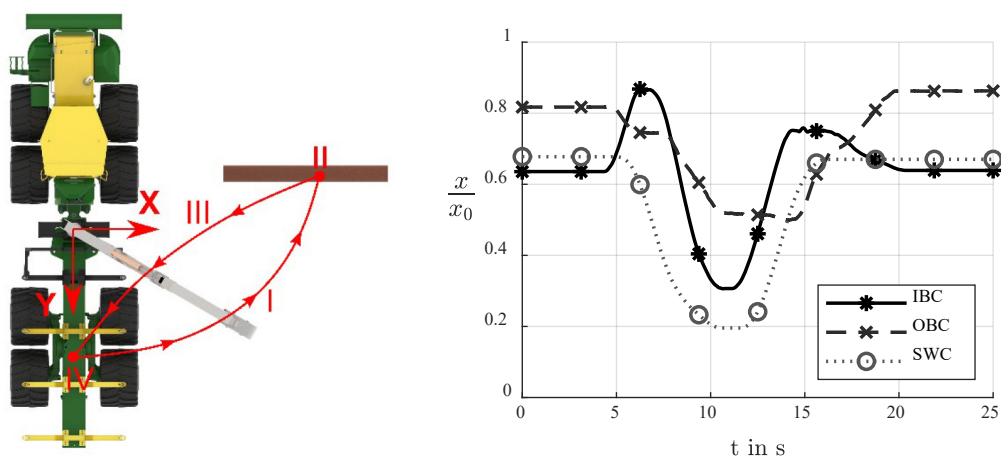


Figure 5: Representation of reference cycle according to GEIGER and GEIMER (2017); sequence of working movement (left); travel paths of inner boom cylinder, outer boom cylinder and swivel cylinder (right)

The actuators IBC, OBC and SWC are operated by an open hydraulic circuit with an eBSS according to SCHERER (2015). Figure 6 shows a schematic diagram of the hydraulic circuit. The function drive of conventional control consists of an electro-hydraulically adjustable pump, which is driven at constant speed. The main control block consists of two electrically controlled 8/3-directional valves, which adjust flow rate to actuators OBC and SWC. The metering edges pump – actuator connection A (PA), pump – actuator connection B (PB), actuator connection A – tank (AT) and actuator connection B – tank (BT) are controlled simultaneously due to a common valve spool. The IBC piston chamber is connected either to pump or tank by an electrically controlled 4/3-directional valve. The rod-side connection of IBC is connected directly to tank line, which is preloaded by 5 bar. The pump connection of all directional valves is equipped each with a pressure compensator valve downstream of the main metering edge (Figure 6). The pressure compensator valve compares local load pressure per actuator with highest load pressure reported by LS line. Together, the pressure compensator valves ensure load-independent control of pump flow rate to all actuators and an even flow rate reduction for all actuators during undersupplied system. The actuators are directly connected to the main control block.

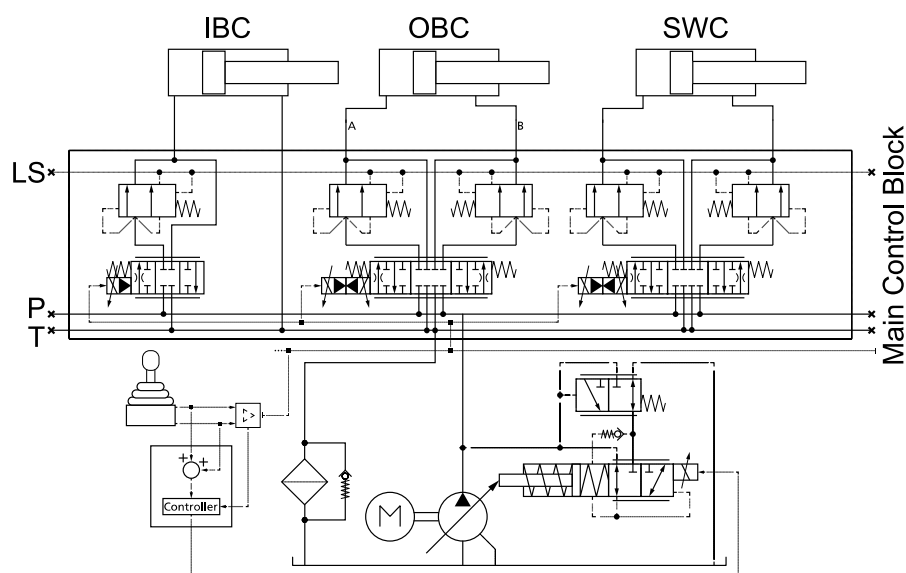


Figure 6: Hydraulic circuit of a forestry crane with an eBSS according to SCHERER (2015); named conventional control

For this investigation, the conventional control system was mapped virtually using the MOBIL method (WYDRA et al. 2018). The 1D simulation model consists of a coupled multi-body simulation (MBSim) of the forestry crane, in common with a hydraulic simulation (HSim) and a control simulation (SSim). The MBSim model was created and validated with Matlab Simulink within the research project Forwarder2020. For the HSim, an eBSS was built and parameterized with the program DSHplus. The SSim represents the investigated control strategies conventional control, reference control and ANN control. The following simplifications apply to the simulation model:

- The pump is driven at a constant speed.
- The dynamics of directional valves are described by PT1 element.
- Dynamic influences by fittings, pipes and hoses are neglected and only shown as capacities between two elements (valves, pump, etc.).

- The grapple, telescope and rotary drive are not operated during a loading cycle.
- The control strategies conventional control, reference control and ANN control are only applied to OBC, as this cylinder represents the changes associated with different control strategies. On one hand, in contrast to the SWC, the OBC is continuously controlled during loading cycle in the majority of cases. On other hand, by substituting the 8/3-directional control valve into two 4/3-directional control valves, the changes are easier to understand than on IBC, which rod-side connection has no valve.
- A change in load caused by picking up the log during loading cycle is not considered, as the load is supported significantly on IBC due to crane kinematics. Internal tests have shown that the pressure in IBC is increased by approx. 13 bar to 37 bar and in OBC by approx. 1 bar to 19 bar during a movement under load of a 300 kg log weight.

The schematic of overall simulation is depicted in Figure 7. Recorded current values I_{IBC} , I_{SWC} are used as control signals for the actuators IBC and SWC. These are converted into a valve spool displacement y_{IBC} , y_{SWC} . Afterwards these signals are transformed by a PT1 element and finally passed on to the metering edges of the directional valves, which are designed as orifices.

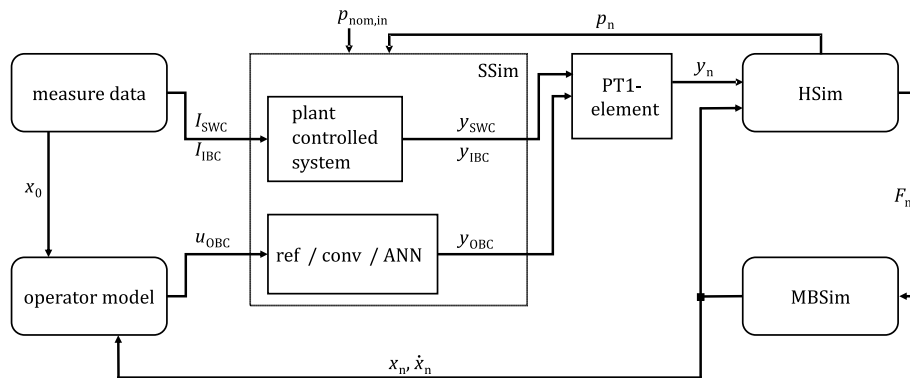


Figure 7: Structure of the overall simulation and signal flow between blocks

For OBC an operator model according to THIEBES and VOLLMER (2011) is implemented. The operator model calculates a control signal for SSim. This control signal u_n can in reality be interpreted as a joystick signal. In eBSS systems flow rate is set by control signal directly, which correlate with a percentage value of maximum flow rate $Q_{n,max}$. The operator model has already been used by SCHERER (2015) and WYDRA et al. (2017) to operate actuators in eBSS systems. The control signal u_{OBC} calculated by the operator model is processed by SSim model into valve spool displacement y_{OBC} and forwarded via PT1 element to metering edges AT_{OBC} , PA_{OBC} , PB_{OBC} and BT_{OBC} , of the outer boom cylinder directional valve. The metering edges are modelled as orifices. The HSim calculates pressures p_n and actuator forces F_n . This is done using cylinder paths x_n and cylinder speeds \dot{x}_n calculated by MBSim and valve spool displacements y_n from SSim.

Modification of conventional system

WEISS and WYDRA (2019) describe how eBSS can be equipped with separate metering edges by modifying directional valves of the main control block. Independent metering between actuators inlet and outlet was achieved by installing two 4/3-directional valves per actuator instead of one 8/3-directional valve (Figure 8, left). This enables a new degree of freedom in system control. In order to

reduce resulting complexity, the metering edges PA and AT as well as PB and BT are selected in such a way that geometrically the same relationship between valve spool displacement $y_{A/B}$ and metering edges flow surfaces $A_{P/T}$ ($V_{A/B}$) exists. In Figure 8 (right), this modification between the system with conventional control (SCHERER 2015) and with reference control (WEISS und WYDRA 2019) is shown.

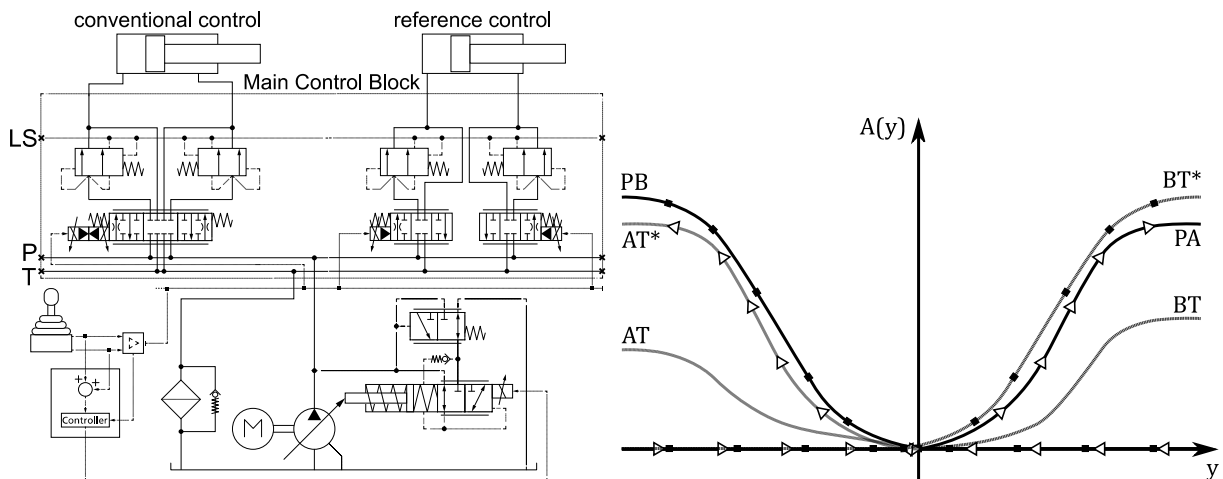


Figure 8: Replacement of the 8/3-directional valve by two separately controllable 4/3-directional valves (left); according to WYDRA et al. (2017); Adjustment of metering edges flow surface (right)

The control strategy according to WYDRA et al. (2017) enables operating an actuator with both passive and active loads securely. The control strategy provides that the meter-in edge is directly controlled by an open loop control. The meter-out edge is set by a pilot operated closed loop control. The pilot control is proportional to the control signal of the meter-in edge. The resulting control behavior corresponds to that of conventional control. Thus, an active load is always handled by the system like a passive load. In parallel, the meter-out edge is continuously opened by regulating pressure on actuator inlet-side, so that the required pump pressure is reduced. Thus, the system is energetically optimized during movement. The control concept is shown in the Figure 9 as a block diagram. This control strategy uses the control signal specified by the operator as input variables u_n , a defined pressure threshold $p_{nom,in,n}$ for actuator inlet-side and the current actuator pressures $p_{A,n}$, $p_{B,n}$ at actuator connections A and B. With this information, the directional valve spool displacement $y_{A,n}$, $y_{B,n}$ of the main control block are calculated. In the HSim model these spool displacements are converted by look-ups into metering edges flows surfaces $A_{AT,n}$, $A_{PA,n}$, $A_{PB,n}$ and $A_{BT,n}$.

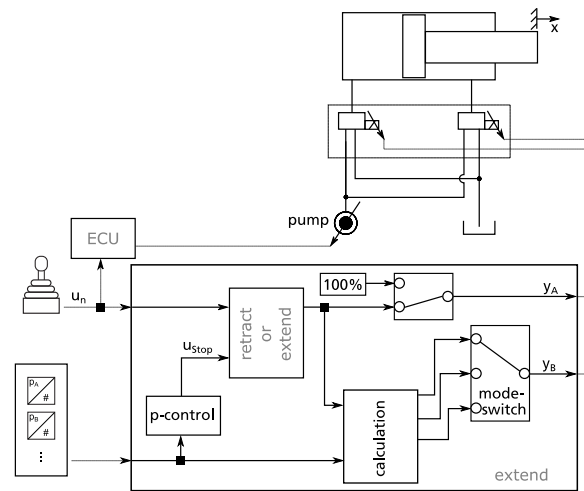


Figure 9: Control structure of the reference control according to WYDRA et al. (2017)

In Figure 10, the result of the control strategy specified in WYDRA et al. (2017) is explained in more detail. The control signals for the inlet and outlet of an actuator on a test rig are shown on the left side. The actuator inlet and outlet pressures are shown on the right side. The conventional control system with coupled metering edges is represented by the blue lines. The reference control system with separate metering edges is represented by the red lines. The hydraulic cylinder extends between second 2 and 5 and retracts between second 7 and 10. During the extending movement, there is a passive load. The control signals of meter-in edge and meter-out edge are proportional. In Figure 10 (left) it can be seen that the meter-out edge $y_{B, HM}$ (red) is opened further than $y_{B, konv}$ (blue). This reduces the required pump pressure for passive loads, Figure 10 (right). During the retracting movement it can be seen that with $y_{A, HM}$ the pilot control initially sets a similar valve spool displacement for the meter-out edge as $y_{A, konv}$. The pressure control leads to an opening of the meter-out edge in the further course of the movement $y_{A, HM}$, Figure 10 (left). From approx. 8.5 s a stationary value is reached. From there, $y_{A, HM}$ is more open than $y_{A, konv}$, which leads to a reduced pump pressure (Figure 10, right).

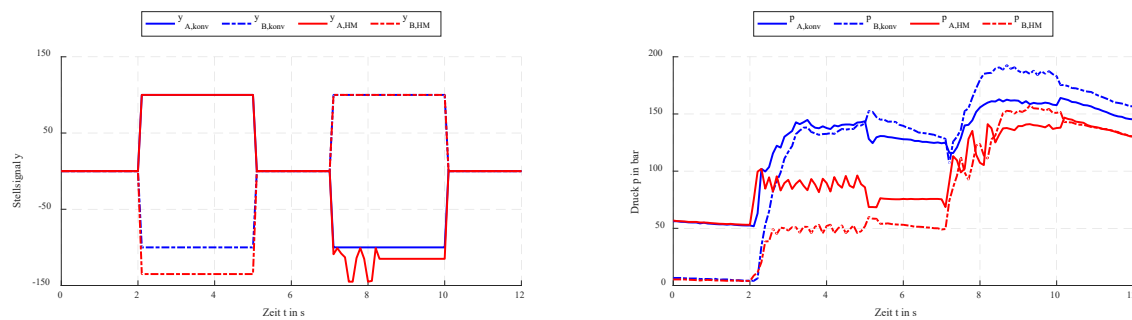


Figure 10: Course of the directional valve spool displacement (left) and the pressure of the actuator ports A/B (right) during extending and retraction of a differential cylinder for conventional control (blue) and reference control (red) (WEISS and WYDRA 2019)

Method for creating the artificial neural network

After the hydraulic system has been presented, this and the following sections describe the procedure as well as the results for imitating and optimizing using artificial neural networks (ANN). A combination of supervised and reinforcement learning is applied for creation and training the ANN. The process is shown in Figure 11. Supervised learning is used to train the ANN to target behavior. This is done using training data consisting of input and output data of the reference control system. To generate training data, systematically varied input data, which are specified in the entire parameter range of the reference control, are simulated. Then, the output data are recorded. The primary goal is to determine suitable network parameters and initial weights. The network parameters sought are the number of hidden layers and the number of neurons per layer.

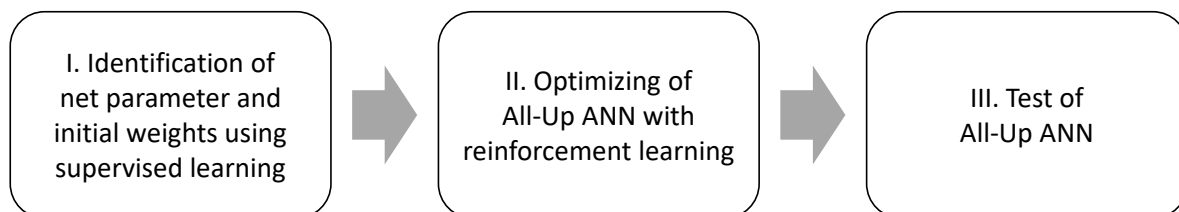


Figure 11: Sequence for creating ANN control

While reinforcement learning, step-by-step changes are made to the weights of the All-Up ANN. With each change, a new simulation is run and its results are evaluated positively or negatively (GOODFELLOW et al. 2018). More detailed explanations of combination of two learning methods as well as advantages and disadvantages are introduced by BLUME and JAKOB (2009).

Identification of network parameters with supervised learning

The control strategy according to WYDRA et al. (2017) uses closed-control loops. To be able to map closed-control loops, the ANN needs a time response. This can be realized, for example, via external, time-delayed feedback (BERNS 1994). A feedback of many neurons leads to a large number of parameters. The theoretical time needed to identify the optimal weights grows exponentially with the number of weights. Thus, as few feedbacks as possible are used.

To achieve this, the entire control task is divided into small, separate and independent subtasks. For each subtask a separate Sub-ANN is trained. The individual Sub-ANN are then put together and considered as one All-Up ANN. The control task can therefore be executed by an All-Up ANN with a small number of parameters. This has a positive effect on computing time required for optimization during later reinforcement learning. Figure 12 shows the procedure for creating a structure-optimized Sub-ANN by supervised learning. Steps 1) to 3) are first created manually by analysis the control strategy to be imitated. In this case, the reference control. The output and input data of the reference control are scaled to a range from -1 to 1 for each Sub-ANN according to its maximum and minimum data. In steps 4) and 5), network parameters of the Sub-ANN are automatically increased step by step until the error square between training data and results of Sub-ANN is less than 0.02% of maximum starting value. Overfitting of individual Sub-ANN initially is irrelevant, since weights of the All-Up ANN are changed in further course of optimization.

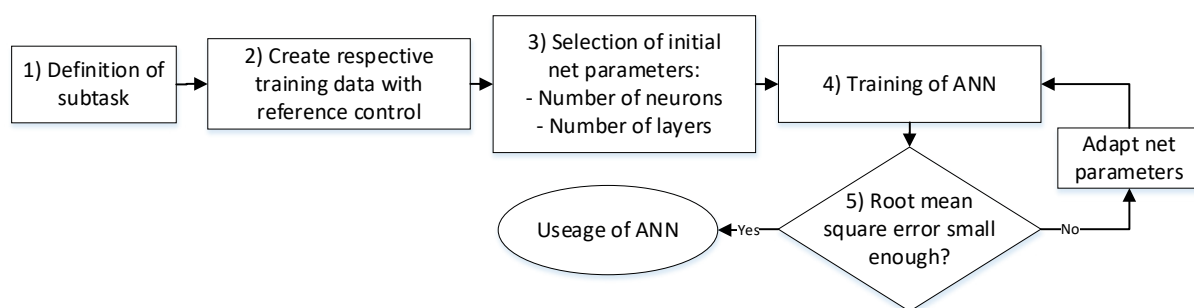


Figure 12: Procedure for supervised learning according to BAUER (2019)

Classical Feedforward Multi-Layer Perceptron (MLP) networks are used as Sub-ANN. A Tansig activation function is used in the first hidden layers. A linear activation function is used in the last hidden layer. A weighted sum with absolute terms is used in all hidden layers to determine the potential (MIKUT 2008). The number of training data per network and resulting network parameters are listed in Table 1.

Table 1: Final data of the Sub-ANN

	Sub-ANN 1	Sub-ANN 2	Sub-ANN 3
Inputs Sub-ANN	Δp time-delayed output of Sub-ANN 1	Δp Output Sub-ANN 1	Q_{nom} Output Sub-ANN 2
Number of training data	316,201	316,201	56,481
Number of neurons hidden layer 1	2	2	4
Number of neurons hidden layer 2	1	1	1
Error square related to maximum output quantity	$2.854 \cdot 10^{-12}$	$1.869 \cdot 10^{-10}$	$2.757 \cdot 10^{-9}$

The resulting All-Up ANN for mapping the reference control is shown schematically in Figure 13. The All-Up ANN consists of three Sub-ANN with each two hidden layers. Together they contain 11 neurons. In total there are 28 weights.

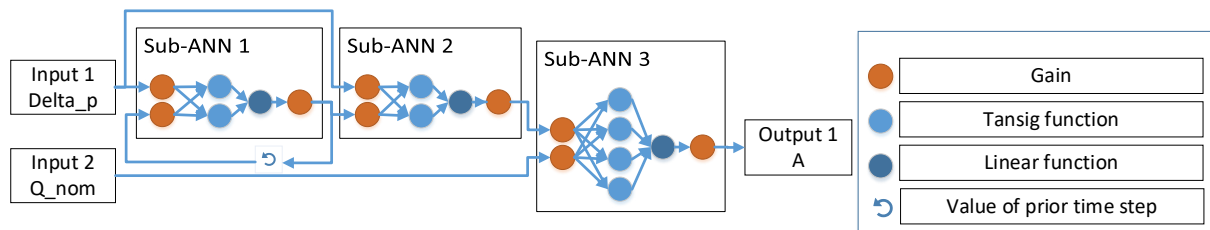


Figure 13: Structure of All-Up ANN control consisting of several Sub-ANN

Optimization of artificial neural network with reinforcement learning

To optimize the All-Up ANN, its weights are iteratively changed with the Pattern-Search algorithm according to Figure 14. The target variables to be optimized are the required pump energy E per cycle and the control deviation γ . This describes the deviation between nominal and actual velocity of the actuator. Details of the algorithm used are described in MATHWORKS (2019a, b). The change of weights is determined by an iterative evaluation of the overall system like described by BAUER (2019). Each generation consists of a parameter set of weights.

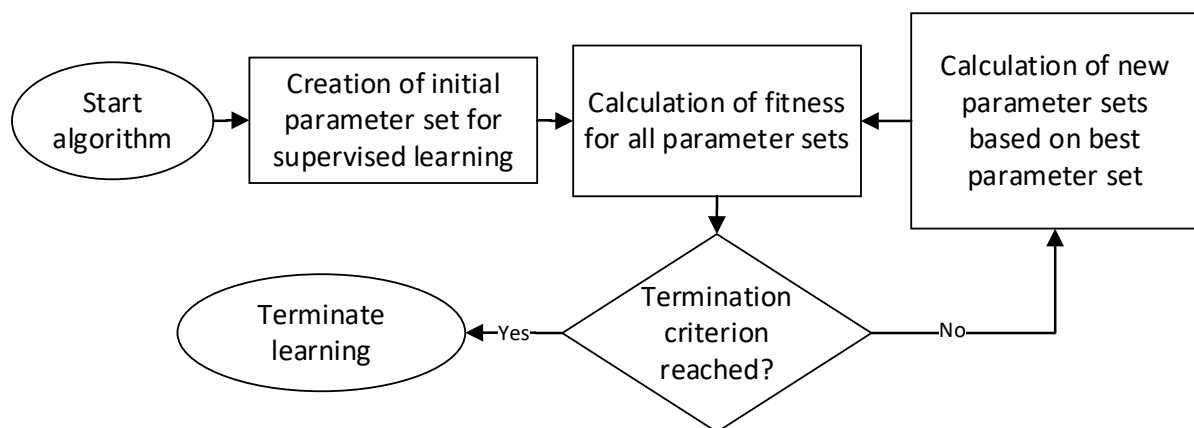


Figure 14: Sequence of reinforcement learning using the Pattern-Search algorithm according to BAUER (2019)

The entire system is simulated with six different optimization cycles for each parameter set. Each optimization cycle is evaluated with regard to its energy consumption E and its control deviation γ . The energy consumption on the hydraulic side is calculated by integration of necessary pump power (Equation 3).

$$E = \int P_p dt = \int \Delta p_p \cdot Q_p dt \tag{Eq. 3}$$

The control deviation γ is calculated as the total difference between nominal and actual velocity of an actuator (Equation 4).

$$\gamma = \int v_{nom} - v_{actual} dt \tag{Eq. 4}$$

The All-Up ANN control uses the control signal u_n and the actuator pressure of the meter-out edge Δp_{out} . To be able to optimize a control system without the influence of an operator, six manually generated control signals are specified. The six optimization cycles give different target velocities between 0 and 100% of maximum velocity v_{max} . The velocity profiles of the training cycles are shown in Figure 15.

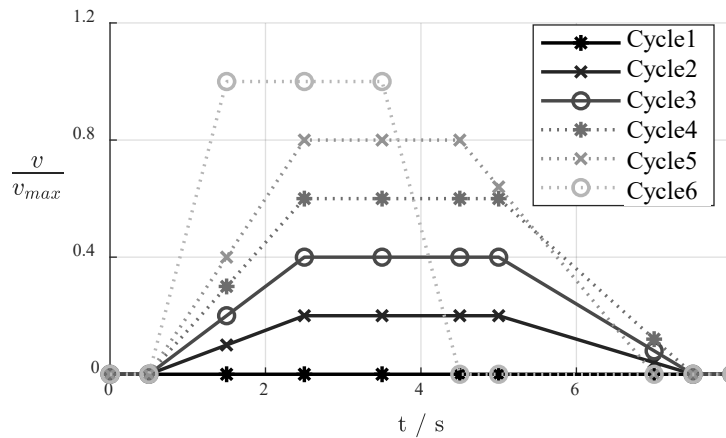


Figure 15: Preset control signals of the six optimization cycles

Four criteria are considered to evaluate the parameter sets. If these criteria are fulfilled, the parameter set will be positively evaluated and thus further optimized. On one hand side, it is considered what improvements are achieved in the overall system due to a changed parameter set. For this purpose, the sum of the energy consumption E_i as well as the control deviation γ_i for all of the six optimization cycles are considered. Thus, the following two conditions result:

- The total energy consumption of the current parameter set is less than the total energy consumption of the best parameter so far (Equation 5).

$$\sum_{i=1}^6 E_i < \sum_{i=1}^6 E_{i,best} \tag{Eq. 5}$$

- The total control deviation of the current parameter set is at most 2% greater than the total control deviation achieved by the initial parameter set (Equation 6)

$$\sum_{i=1}^6 \gamma_i \leq \sum_{i=1}^6 (\gamma_{i,0}) \cdot 1,02 \quad (\text{Eq. 6})$$

In order to prevent the All-Up ANN from being overfitted in some areas while the system behavior deteriorates in other operating areas, the energy consumption or control deviation from each individual optimization cycle is also considered. The energy consumption E_i in each of the six optimization cycles must not exceed 5% of the energy consumption $E_{i,\text{best}}$ which was achieved by the best parameter set in the respective optimization cycle (Equation 7).

$$E_i \leq E_{i,\text{best}} \cdot 1,05; i = 1 \dots 6 \quad (\text{Eq. 7})$$

- The control deviation γ_i in each of the six optimization cycles must not exceed 2% of the control deviation $\gamma_{i,0}$, which was achieved by the initial parameter set for the respective optimization cycle (Equation 8).

$$\gamma_i \leq \gamma_{i,0} \cdot 1,02; i = 1 \dots 6 \quad (\text{Eq. 8})$$

For the optimization 41 generations of parameter sets were calculated on an institute-owned computer. Table 2 shows the system data for the computer used for optimization. The total calculation time was 90 hours.

Table 2: System data of the computer used to optimize the All-Up ANN

Operating system	Number of processors	Processor type	Clock frequency in GHz	Number of processor cores per processor	Working memory in GB
Windows Server 2008 R2 Enterprise	2	Intel Xenon CPU X5680	3,33	6	48

Results of optimization with reinforcement learning

Figure 16 shows for each generation the sum of the energy consumption (training fitness), which is caused by the six optimization cycles for best individual of the respective generation. The result has improved by approx. 14.6% after 41 generations. Figure 16 shows, that the greatest improvement occurred between 6th and 12th generation. A further significant improvement can be seen between 20th and 25th generation. When major improvements will occur and whether the parameter set found in Generation 41 is the best solution, cannot be clearly identified due to the black box properties of an ANN.

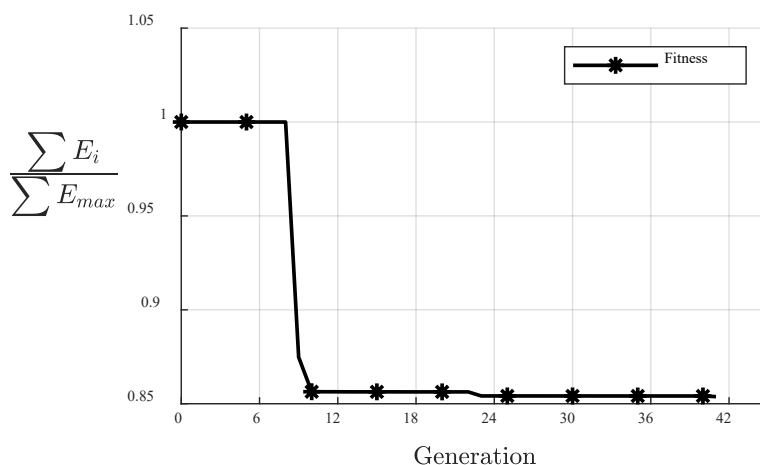


Figure 16: Development of energy consumption over generations of parameter sets

Figure 17 shows the relative energy consumption for the individual optimization cycles E (left) and the relative control deviation γ (right) of the control system with initial and optimized parameter set for the All-Up ANN. A maximum reduction of total energy consumption by $\Delta E \approx 14.6\%$ compared to the initial All-Up ANN control can be achieved for the optimization cycles. It can be seen that the energy consumption shows an improvement at each optimization cycle. The total control deviation is reduced on average by $\Delta\gamma \approx 4.33\%$.

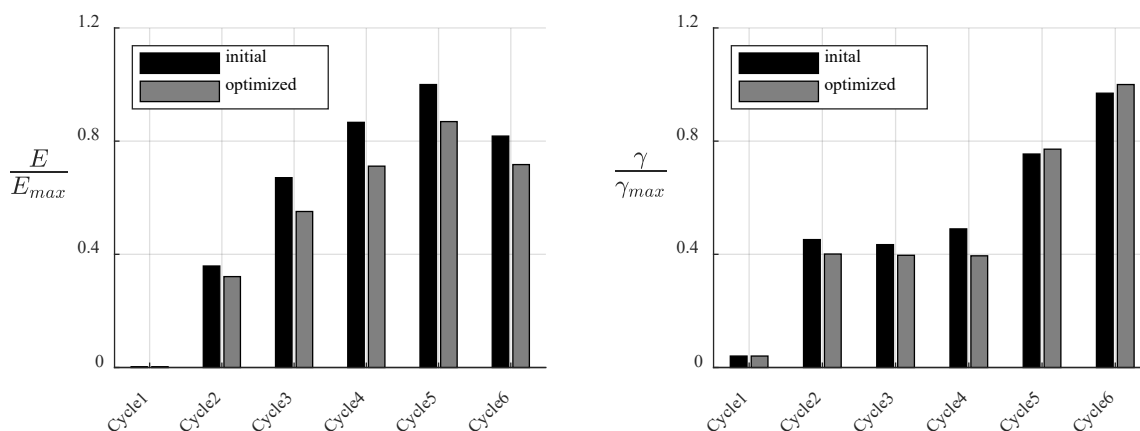


Figure 17: Relative energy consumption E regarding the maximum energy consumption of all values E_{max} (left); relative control deviation γ with regard to the maximum control deviation of all values γ_{max} for all six optimization cycles (right)

During the training of ANN overfitting is possible for various reasons (GOODFELLOW et al. 2018). An overfitting can be checked by using the All-Up ANN under several test conditions and using the same evaluation criteria for comparison. For this reason, the optimized All-Up ANN control system is tested on eleven test cycles, which represent as heterogeneous operating areas as possible. This time, the test cycles consist of defined path trajectories, which are run by an operator model (Figure 18). The path trajectories are selected in such a way that the resulting target velocities differ from the training cycles.

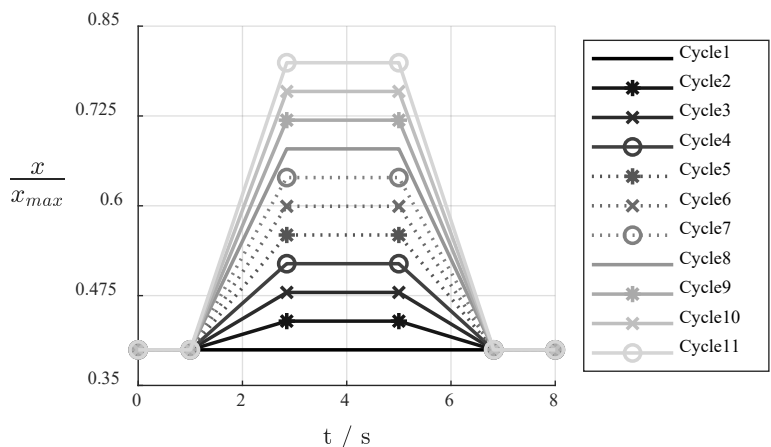


Figure 18: Test cycles as default for the operator model to check whether there is an overfitting of the All-Up ANN

Figure 19 shows the energy consumption E and the control deviation γ of the All-Up ANN control systems with initial and optimized parameter set for all eleven test cycles. In all eleven test cycles, the total energy consumption of the optimized All-Up ANN control system is on average reduced by $\Delta E \approx 14.44\%$ compared to the initial All-Up ANN control system. The total control deviation could be reduced on average by $\Delta \gamma \approx 8.13\%$ compared to the initial All-Up ANN control system. The energy consumption of the system with optimized parameter set is in none of the eleven test cycles worse than with initial parameter set. The control deviation of the system with optimized parameter set is better than initial parameter set in five of eleven test cycles, worse than initial parameter set in four of eleven test cycles and equal to initial parameter set in two of eleven test cycles. The authors judge that the optimized parameter set of the All-Up ANN is sufficiently trained due to the results that there is no overfitting.

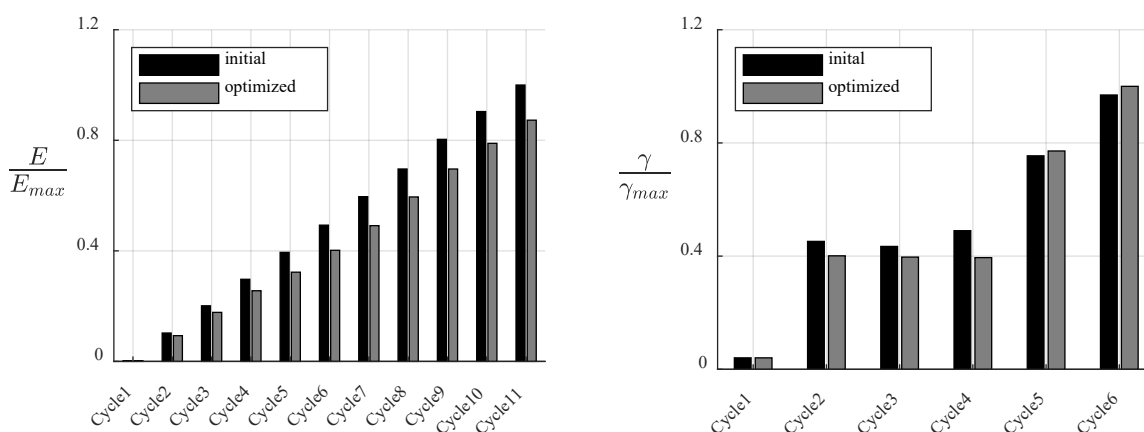


Figure 19: Relative energy consumption E regarding the maximum energy consumption of all values E_{max} (left); relative control deviation γ regard to the maximum control deviation of all values γ_{max} for all eleven test cycles (right)

Comparison of conventional control, reference control and optimized all-up ANN control

The controllability and energy requirements of all three control systems - conventional control (conv), reference control (ref) and All-Up ANN control (ANN) - are discussed below. The controllability is determined by the relative deviation between nominal and actual trajectory of the outer boom cylinder $\Delta x_{OBC,s}$ (Equation 9).

$$\Delta x_{OBC,s} = \frac{(x_{nominal} - x_s)}{x_{nominal}}; s = conv, ref, ANN \tag{Eq. 9}$$

The relative deviation between nominal and actual trajectory is on average for the conventional control systems $\Delta x_{OBC,conv} = (0,6 \pm 11)\%$, for the reference control $\Delta x_{OBC,ref} = (0,6 \pm 10)\%$ and for the All-Up ANN control $\Delta x_{OBC,ANN} = (-0,2 \pm 4)\%$. The paths x_s relative to the total extension length of the outer boom cylinder x_0 are shown in the upper diagram of Figure 20. For a better representation, the lower diagram of Figure 20 shows the relative deviations of actual to nominal trajectory in relation to the total extension length of the outer boom cylinder x_0 in %.

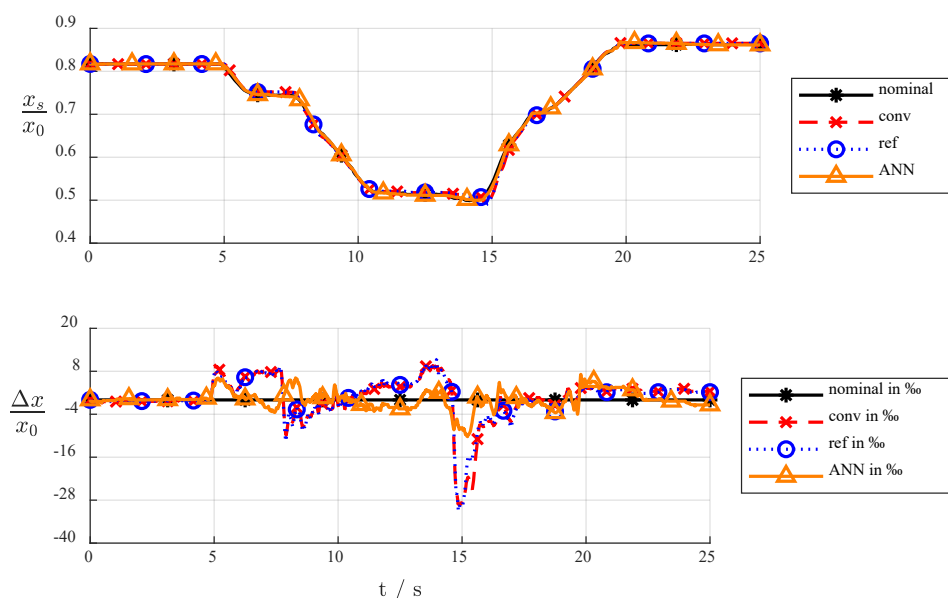


Figure 20: Relative path of the outer boom cylinder when using the conventional control system (conv) (top), the reference control (ref) and the optimized ANN control; relative deviation of target and actual trajectory Δx to the total extension length of the outer boom cylinder x_0 (bottom)

To illustrate the reasons for an increase in energy efficiency, the p - Q timeline of the pump is compared in Figure 21. The pressure is related to the maximum system pressure p_{max} . The flow rate is related to the maximum pump flow rate Q_{max} at a fixed speed n . It can be seen that the reference control as well as the ANN control system reduce the pressure level by an average of approx. $\Delta p_{ref} = -2,7$ MPa (7,9%) respectively $\Delta p_{ANN} = -2,5$ MPa (7,2%). At an approximately equal flow rate with an average deviation of $\Delta Q_{ref} = 1,1\%$ respectively $\Delta Q_{ANN} = 1,3\%$ to conventional control, the necessary power of the system is reduced.

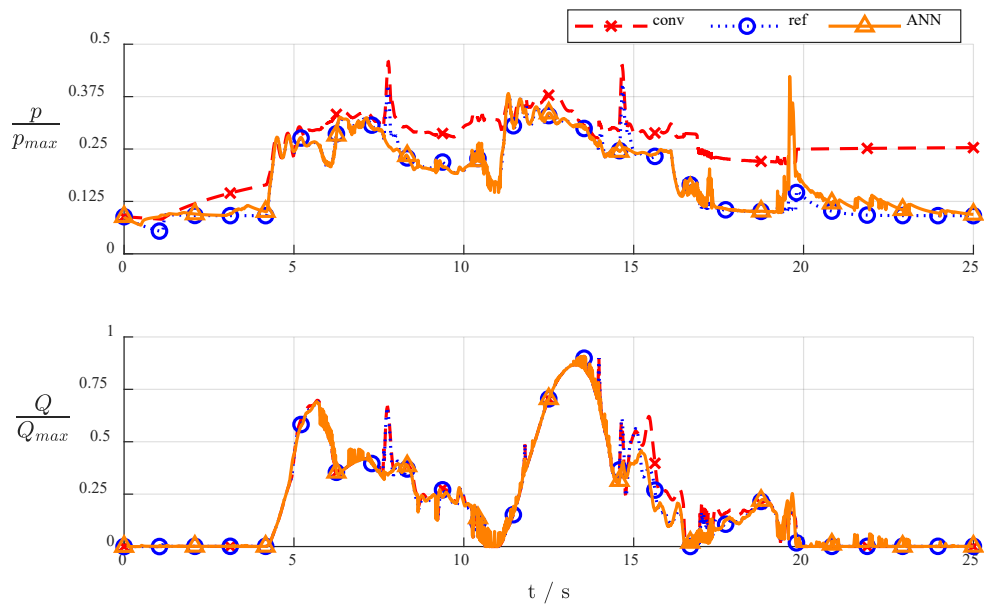


Figure 21: Curves for the pump pressure (top); curves for the pump flow rate (bottom)

The result of the reduced pressure level can be seen in the power and energy requirements of the pump (Figure 22). The power and energy are limited to the maximum power $P_{conv,max}$ and energy $E_{conv,max}$ of the conventional control system. Between approx. 7 and 10 s as well as approx. 14 and 16 s it can be seen that the pump power required for the reference and All-Up ANN control is lower than for conventional control system. This difference becomes particularly obvious when looking at the energy. At the end of a reference cycle, the energy difference of the reference control in relation to the conventional control is $\Delta E_{ref} = -18,7\%$ and those of the All-Up ANN control $\Delta E_{ANN} = -20,5\%$.

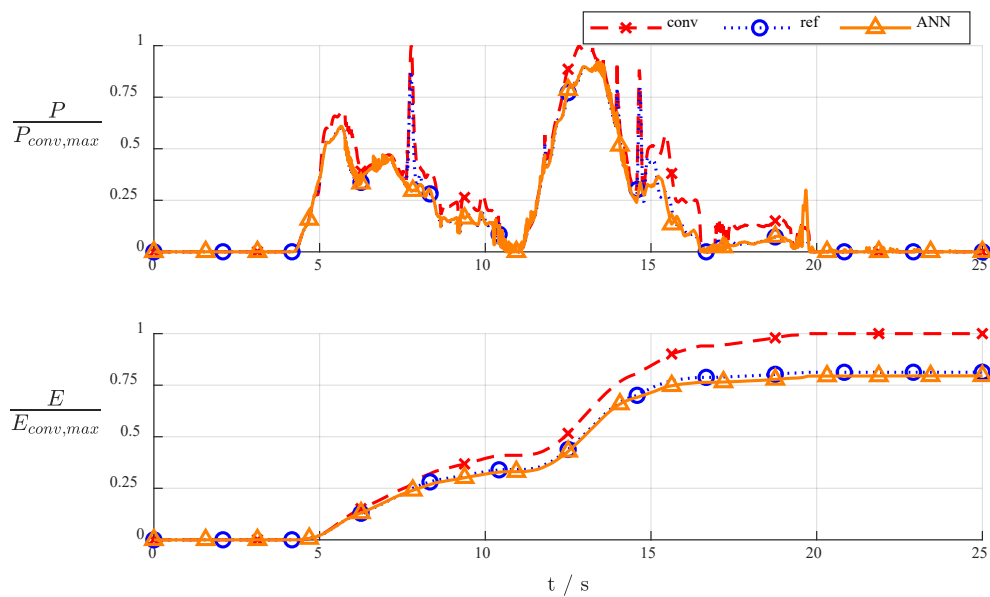


Figure 22: Curve of the hydraulic pump power (top); sum of the required hydraulic pump energy (bottom)

Conclusions

Finally, there are well researched solutions ready-to-use, which offer significant advantages in energy efficiency and controllability compared to existing state of the art solutions. Furthermore, this contribution shows that existing complex control algorithms can be imitated by artificial neural networks (ANN) and subsequently optimized.

By applying the control algorithms to the function drive of a forestry crane, it could be shown that the control strategy of an existing electro-hydraulic flow-on-demand control with independent metering (reference control) can be represented by an ANN. This ANN control, with the current state of optimization, does not show any significant improvement or deterioration of energy efficiency or control quality compared to the reference control. For this paper 41 generations of parameter sets were generated using the Pattern Search algorithm. Therefore, it cannot be excluded that further runs could lead to a significant improvement. If this would be the case, this method offers the possibility to map and optimize other, existing control algorithms as ANN. It should be mentioned that this method does not have self-learning properties due to the required training data. Therefore, this method cannot be used for unknown systems.

It still remains unexplored,

- how to generate full self-learning control algorithms for electro-hydraulic drives.
- which behavior the generated All-Up ANN control shows in non-tested test scenarios and cycles.
- whether it is possible to adapt the generated All-Up ANN control to different power classes of forestry cranes with the same systemic structure by applying the reinforcement learning process.
- whether applying the presented method to other control strategies and machines will lead to comparable results.

References

- Altenburg, S.; Maur, A. auf der; Labinsky, A.; Eckert, S.; Faltenbacher, M.; Reuter, B. (2017): Nullemissionsnutzfahrzeuge. Vom ökologischen Hoffnungsträger zur ökonomischen Alternative. Studienbericht, Stuttgart, e-mobil BW GmbH
- Axin, M. (2013): Fluid power systems for mobile applications. With a focus on energy efficiency and dynamic characteristics. Dissertation, Linköping, Linköping University, Department of Management and Engineering
- Backé, W.; Baum, H. (2013): Systematik fluidtechnischer Schaltungen. Theoretische Einführung und Simulation von Praxisbeispielen, Aachen, Shaker Verlag
- Bauer, A. (2019): Einsatz neuronaler Netze zur Steuerung von elektrohydraulischen Ventilen. Masterthesis, Karlsruher Institut für Technologie (KIT)
- Berns, K. (1994): Steuerungsansätze auf der Basis neuronaler Netze für sechsbeinige Laufmaschinen. Dissertation, Sankt Augustin, Infix
- Blume, C.; Jakob, W. (2009): GLEAM – General Learning Evolutionary Algorithm and Method. Ein evolutionärer Algorithmus und seine Anwendungen, Karlsruhe, KIT Scientific Publishing
- Buxmann, P.; Schmidt, H. (2019): Künstliche Intelligenz. Mit Algorithmen zum wirtschaftlichen Erfolg, Berlin, Heidelberg, Springer, <https://doi.org/10.1007/978-3-662-57568-0>
- Dengler, P. (2015): Untersuchung zum effizienten Betrieb von Hydraulikzylindern in Konstantdrucksystemen unter Verwendung einer Zwischendruckleitung. Dissertation, Karlsruhe, KIT Scientific Publishing, <https://doi.org/10.5445/KSP/1000043836>
- Eriksson, B. (2010): Mobile fluid power systems design. With a focus on energy efficiency. Dissertation, Linköping, LiU-Tryck

- Esders, H. (1996): Elektrohydraulisches load sensing für mobile Anwendungen. Dissertation, Düsseldorf, VDI-Verl.
- Findeisen, D. (2006): Ölhdraulik, Berlin, Heidelberg, Springer, <https://doi.org/10.1007/3-540-30967-5>
- Geiger, C.; Geimer, M. (2017): Efficiency Optimisation of a Forestry Crane by Implement Hydraulics with Energy Recovery. In: Land.Technik AgEng 2017, Conference Agricultural Engineering; Max-Eyth-Gesellschaft für Agrartechnik; Landtechnik AgEng, 10.-11.11.2017, Hannover, VDI Verlag, S. 175–184, <https://doi.org/10.5445/IR/1000077237>
- Geimer, M.; Pohlandt, C. (2014): Grundlagen mobiler Arbeitsmaschinen, Karlsruhe, KIT Scientific Publishing, <https://doi.org/10.5445/KSP/1000039443>
- Goodfellow, I.; Bengio, Y.; Courville, A. (2018): Deep Learning. Das umfassende Handbuch. Grundlagen, aktuelle Verfahren und Algorithmen, neue Forschungsansätze, Frechen, mitp Verlags GmbH & Co. KG
- Hänel, F.; Rautenberg, H.; Kunze Günter (2015): Gefährdung durch Feinstaubemissionenvon Baumaschinen. Studie, Frankfurt, Forschungsvereinigung Bau- und Baustoffmaschinen e. V.
- Kolks, G.; Weber, J. (2016): Modiciency – Efficient industrial hydraulic drives through independent metering using optimal operating modes. In: 10th International Fluid Power Conference, 08.–10.03.2016, Dresden, Dresdner Verein zur Förderung der Fluidtechnik e. V. Dresden, S. 105–120
- Manner, J.; Palmroth, L.; Nordfjell, T.; Lindroos, O. (2016): Load level forwarding work element analysis based on automatic follow-up data. *Silva Fennica* 50(3), <https://doi.org/10.14214/sf.1546>
- MathWorks (2019a): How Pattern Search Polling Works. https://de.mathworks.com/help/gads/how-pattern-search-polling-works.html?searchHighlight=how%20patternsearch&s_tid=doc_srchtile, accessed on 10 Dec 2019
- MathWorks (2019b): patternsearch. https://de.mathworks.com/help/gads/patternsearch.html?searchHighlight=patternsearch&s_tid=doc_srchtile, accessed on 10 Dec 2019
- Mikut, R. (2008): Data Mining in der Medizin und Medizintechnik. Teilw. zugl.: Karlsruhe, Univ., Habil.-Schr., 2007 u.d.T.: Mikut, Ralf: Automatisierte Datenanalyse in der Medizin und Medizintechnik, Karlsruhe, Universitätsverlag
- Pohlandt, C. (2018): Intelligentes Gesamtmaschinenmanagement für elektrische Antriebssysteme. Dissertation, Karlsruhe, KIT Scientific Publishing, <https://doi.org/10.5445/KSP/1000081063>
- Renius, K.T. (2019): Fundamentals of tractor design, Cham, Springer, <https://doi.org/10.1007/978-3-030-32804-7>
- Rocca, W. (2003): Lasten sicher im Griff. Zweistufiges-Senkbremsventil mit konstantem und degressivem Gegendruck. *Fluid* 37, S. 8–11
- Scherer, M. (2015): Beitrag zur Effizienzsteigerung mobiler Arbeitsmaschinen. Entwicklung einer elektrohydraulischen Bedarfsstromsteuerung mit aufgeprägtem Volumenstrom. Dissertation, Karlsruhe, KIT Scientific Publishing, <https://doi.org/10.5445/KSP/1000045508>
- Steindorff, K. (2010): Energierückgewinnung am Beispiel eines ventilgesteuerten hydraulischen Antriebs. Dissertation, Aachen, Shaker Verlag
- Thiebes, P.; Vollmer T. (2011): Modellierung des Fahrers zur Untersuchung von Antriebssträngen in der 1D-Simulation am Beispiel eines Radladers mit Hybridantrieb. In: 3. Fachtagung Hybridantriebe für mobile Arbeitsmaschinen, Lehrstuhl für Mobile Arbeitsmaschinen (Mobima), 17.02.2011, Karlsruhe, KIT Scientific Publishing, S. 47–59
- Vukovic, M.; Leifeld, R.; Murrenhoff, H. (2017): Reducing Fuel Consumption in Hydraulic Excavators—A Comprehensive Analysis. *Energies* 10(5), S. 687, <https://doi.org/10.3390/en10050687>
- Weiss, B.; Wydra, M. (2019): Elektrohydraulische Bedarfsstromsteuerung mit Hybridfunktion zur Steigerung der Energieeffizienz von Forstmaschinen. Abschlussbericht, Osnabrück, Deutsche Bundesstiftung Umwelt – DBU
- Wydra, M.; Geimer, M.; Weiss, B. (2017): An Approach to Combine an Independent Metering System with an Electro-Hydraulic Flow-on-Demand Hybrid-System, 07.–09.07.2017, Linköping, Sweden, Linköping University Electronic Press, S. 161–170, <https://doi.org/10.5445/IR/1000072317>
- Wydra, M.; Siebert, J.; Weiß, B.; Geimer, M. (2018): Entwicklung einer Kransteuerung auf Basis der MOBIL-Methode. In: 10. Kolloquium Mobilhydraulik, Institut für mobile Maschinen und Nutzfahrzeuge (IMN), Technische Universität Braunschweig, 16.–17.10.2018, Braunschweig, Institut für mobile Maschinen und Nutzfahrzeuge (IMN), S. 1–12, <https://doi.org/10.5445/IR/1000096002>

Zhang, S.; Minav, T.; Pietola, M.; Kauranne, H.; Kajaste, J. (2019): The effects of control methods on energy efficiency and position tracking of an electro-hydraulic excavator equipped with zonal hydraulics. *Automation in Construction* 100, S. 129–144, <https://doi.org/10.1016/j.autcon.2019.01.003>

Authors

Marco Wydra (M. Sc.), **Chris Geiger (M. Sc.)** are academic researchers, **Andreas Bauer (M. Sc.)** is a research assistant and **Prof. Dr.-Ing. Marcus Geimer** is head of the Institute of Mobile Machines (Mobima) at Karlsruhe Institute of Technology (KIT), Rintheimer Querallee 2, 76131 Karlsruhe. E-mail: marco.wydra@kit.de

Acknowledgements

Parts of this article are taken from the project Forwarder2020. This project was financed under the grant agreement no. 727883 from the European Union's Horizon 2020 research and innovation program.

Parts of this paper are taken from the project Elektrohydraulische Bedarfsstromsteuerung mit Hybridfunktion zur Steigerung der Energieeffizienz von Forstmaschinen. This project was funded by the Deutsche Bundesstiftung Umwelt (DBU), reference number AZ 32624/01.

The authors would like to thank Fluidon Gesellschaft für Fluidtechnik mbH for providing the program DSHplus.